Applied Thermal Engineering 230 (2023) 120704

Contents lists available at ScienceDirect

Applied Thermal Engineering

journal homepage: www.elsevier.com/locate/apthermeng

# Experimental and numerical study on two-phase minichannel cold plate for high-power device

Yifan Zhang [a], Yongxiang Fan [b], Zhichun Liu [a,*], Wei Liu [a]

[a] School of Energy and Power Engineering, Huazhong University of Science and Technology, Wuhan, 430074
[b] CRRC Qingdao Sifang Rolling Stock Research Institute Co. Ltd, Qingdao, 266031

ARTICLE INFO

*Keywords:*
Two-phase flow
High power
Minichannel
Cold plate
Design

ABSTRACT

In this study, the flow and heat transfer performance of the two-phase minichannel cold plates with 10 kW level heat load is designed and studied. The numerical simulation can guide the optimization of the structure on both channel level and whole level, which roughly matches the experimental results. An abnormal phenomenon that the temperature increase with flow rate is observed and explained by boiling point change. The influence of channel structure, fluid characteristics, flow uniformity, and pressure resistance on cold plate temperature and pressure drop are investigated. The fusiform channel performs better than the rectangular channel and refrigerant R1234ze(E) beats R1233zd(E) in the cold plate. Flow uniformity and pressure drop improvement methods are explained and tested. The cold plate can keep its surface temperature below 80 °C and pressure drop below 0.6 bar when the heating power is 20 kW, utilizing R1234ze(E) with a temperature of 60 °C and a flow rate of 9 L/min. A high-power two-phase cold plate can be designed with reference to this study.

## 1. Introduction

With the rapid development of electronic information technology and manufacturing technology, high-power electronic components and equipment are used more and more widely, such as laser diodes array [1], the phased-array antenna [2], IGBT [3], and LED [4]. To make the equipment compact, how to effectively solve the heat dissipation problem of high-power equipment in limited space has gradually become the bottleneck restricting its further development. The achievable heat transfer coefficient of liquid cooling is much bigger than the air cooling system [5]. Liquid cooling systems include direct contact cooling, such as jet impingement and spray cooling, and indirect contact cooling, such as cold plate and heat pipe [6]. This paper mainly studies the cooling of a high-power device with a heat flux of 10 W/cm$^2$ levels and a total heating power of 10 kW level. A two-phase minichannel cold plate is used to match the heat source with the large size, considering the processing economy, surface temperature uniformity, and total flow resistance loss controllability [7].

At present, there is no completely unified criterion to distinguish minichannel in academic circles. Mehendale [8] thinks the hydraulic diameter of the minichannel should be between 100 um to 6 mm, while Kandlikar et al. [9] prefer a range of 200 um to 3 mm. Other researchers are using the dimensionless criterion to distinguish, such as the Co number [10] and Bond number [11]. Because water is safe and cheap, many researchers studied single-phase water cold plates [12]. However, more and more researchers studied the two-phase minichannel cold plate to further improve system compactness and reduce the pump work, mainly through experiments.

Many researchers aimed at getting more accurate, more general prediction correlations to guide the design. Wen et al. [13] experimentally investigated the flow boiling heat transfer of refrigerant R134a in a horizontal multiport minichannel. He proposed a new correlation based on Gungor and Winterton correlation. Strak et al. [14] discussed the applicability of heat transfer correlations to flows in minichannels with different inclination angles, working fluids, and surface characteristics. A dozen or so heat transfer correlations have been compared and a new correlation was proposed with better accuracy. Kizuku et al. [15] developed a novel simulation model which well predicted the flow maldistribution, local quality, heat transfer coefficient, and dry-out region of the two parallel minichannels heated unequally.

But the mechanism of flow boiling is too complex, and a perfect prediction correlation is almost unachievable. Many aspects need to study, such as geometry structure [16–19], operating condition [20–22], gravity [23,24], refrigerants [25,26], nanoparticles [27], surface modification [28,29], flow patterns [30–32], bubble characteristics

* Corresponding author at: 1037 Luoyu Road, Hongshan District, Wuhan 430074, China.
*E-mail address:* zcliu@hust.edu.cn (Z. Liu).

https://doi.org/10.1016/j.applthermaleng.2023.120704
Received 23 September 2022; Received in revised form 5 January 2023; Accepted 3 May 2023
Available online 8 May 2023

**Nomenclature**

*Physical quantity*

| | |
|---|---|
| $D$ | hydraulic diameter (mm) |
| $f$ | fraction factor (-) |
| $F$ | force (N) |
| g | gravity acceleration (m/s$^2$) |
| $h$ | specific enthalpy (J/kg) |
| $H$ | height (mm) |
| $\dot{m}$ | mass transfer rate, (kg/s) |
| $Nu$ | Nusselt number (-) |
| $P$ | pressure (Pa) |
| $Q$ | flow rate (L/min) |
| $q$ | heating power (W) |
| r | thermal resistance (K/W) |
| $R$ | interaction force (N) |
| $T$ | temperature (°C) |
| $u$ | velocity (m/s) |
| $v$ | relative velocity (m/s) |
| $W$ | width (mm) |

*Greek letters*

| | |
|---|---|
| $\alpha$ | phasic volume fractions (-) |
| $\rho$ | density (kg/m$^3$) |
| $\lambda$ | bulk viscosity (Pa·s) |
| $\mu$ | shear viscosity (Pa·s) |
| $\bar{\bar{\tau}}$ | stress–strain tensor (Pa) |

*Subscripts*

| | |
|---|---|
| 0 | reference channel |
| avg | overall average |
| c | channel |
| C | liquid convective |
| E | evaporation |
| exp | experiment |
| f | fin |
| in | inlet |
| l | liquid phase |
| max | maximum |
| out | outlet |
| lv | from liquid phase to vapor phase |
| Q | quenching |
| Sat | saturation |
| simu | simulation |
| v | vapor phase |
| vl | from vapor phase to liquid phase |
| V | vapor convective |
| W | wall |

*Abbreviations*

| | |
|---|---|
| CHF | critical heat flux |
| G | gravity acceleration |
| GWP | global warming potential |
| ODP | ozone depletion potential |
| PEC | performance evaluation criterion |

[33], flow instability [34,35] and some active reinforcement methods [36,37]. Xu et al. [38] made an experimental investigation on a pumped two-phase battery cooling system with R1233zd(E). Along the flow direction, the local temperature was increased and then stabilized, while the local heat transfer coefficient increased monotonously. Liu et al. [39] compared R600a, R227ea, and R245fa in a visualized vertical rectangular minichannel with a cross-section area of 1.6 mm × 10 mm. The experimental results showed that the heat flux and saturation pressure have a significant influence on the heat transfer coefficient, while the effects of the mass flux and vapor quality are negligible. Mastrullo et al. [40] investigated the saturated critical heat flux (CHF) of an aluminum multi-minichannel heat sink with a 1.33 mm inner diameter using R134a, R1234yf, and R1234ze(E). The results showed a general CHF drop with the saturation temperature, especially for lower mass fluxes. Sira et al. [41] experimented with R-134a flowing through a 1 mm inner diameter channel. Different orientations, i.e., horizontal, vertical upward, and vertical downward are tested, revealing the importance of the change in the flow direction. Zho et al. [42] experimentally investigated the effect of activation cavities and analyzed the design parameters. The pressure drops increase with the heat flux at low heat flux conditions and fluctuate intensively at high. Jige et al. [43] experimentally investigated the performance of the zeotropic binary mixture R1234yf/R32 inside horizontal multiport rectangular minichannels. The results show a strong influence of mass flux, vapor quality, and mass fraction on heat transfer, whereas heat flux has a small impact.

Although experiments matter more in flow boiling, numerical simulation still has a place, especially with the explosive advance in computer science recently. It can be used to study novel structures [44], flow patterns [45], flow instabilities [46], bubble characteristics [47], various operating conditions [48], etc. Zhang et al. [49] used a coupled Level-set/Volume of Fluid method to study flow boiling in mini-/microchannels and build a phase change model based on the interfacial temperature gradient. Their simulation results show the transition of flow patterns has a significant influence on heat transfer. Maciejewska et al. [50] used the Trefftz method to determine the heat transfer coefficient on the contact surface between the heated foil and FC-72 in a 1.7 mm deep minichannel. Ma et al. [51] used ANSYS CFX to study a vertical rectangular minichannel and found forced convective boiling governs at high vapor quality and the evaporation of dispersed liquid phase matters.

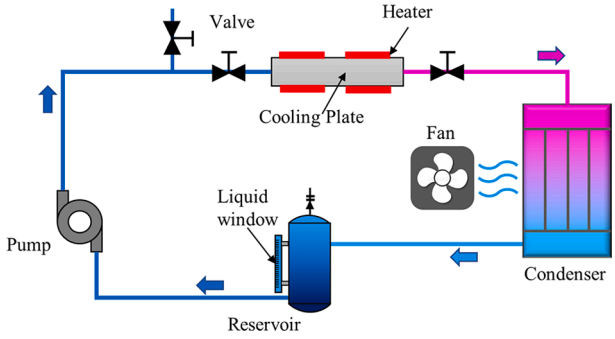


**Fig. 1.** Two-phase cooling system diagram.

Limited by laboratory conditions and computation resources, most researchers focus on one minichannel and small-scale multi-parallel channels. They can achieve high critical heat flux, but the total heating power is limited. When heating power increases a lot, the flow distribution becomes more complex between parallel branches and adds higher requirements for structural design. This paper studies the high-power two-phase flow cold plate with refrigerant R1233zd(E) and R1234ze(E), and the total heat dissipation power is about 10 kW. The numerical simulations of the two-phase cold plate are used to guide the design. At the same time, experiments of the normal and visualized cold plates are carried out to explore the flow characteristics and heat transfer performance. The influence of operating conditions, geometry structure, working fluid, flow uniformity, and pressure loss is well studied.

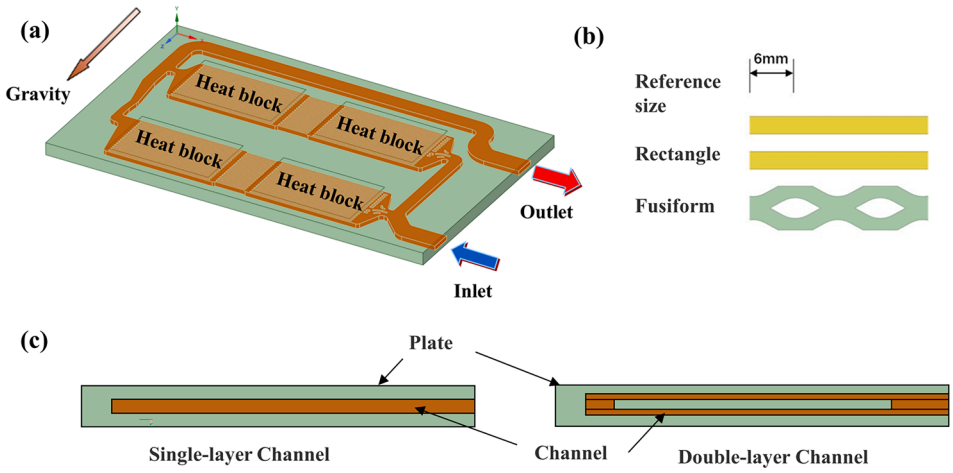


**Fig. 2.** Schematic diagram of (a) the cold plate, (b) its inner channels' structure, and (c) the cross-section of the plate with single-layer or double-layer channels.

## 2. Technical solutions

### 2.1. System

A schematic diagram of the two-phase cooling system is shown in Fig. 1, which includes the cold plate, condenser, reservoir, pump, and several valves. The components are linked by soft aluminum pipelines. A gear pump drives the subcooled working fluid to the cold plate. After heating, partial working fluid evaporates, and the working fluid becomes a two-phase flow. The heated two-phase flow enters the condenser, dissipates heat to the ambient, and becomes subcooled liquid again. A reservoir with adequate volume is set in front of the pump, so it can balance the system pressure and prevent vapor from damaging the pump. So, the pump power the working fluid to circulate, which continually transports heat from the heater to the ambient air.

### 2.2. Cold plate

The cold plate is made of aluminum 6061. Its length, width, and thickness are 560 mm, 355 mm, and 18 mm, respectively. As shown in Fig. 2 (a), the working fluid flows within the cold plate, where eight heating blocks are symmetrically distributed on the front and back. Typically, each heating block will generate 1.25 kW of heat, so the total heat dissipation power is 10 kW. The flow channel is centered in the thickness direction. The total width of the parallel channels on each branch is about 100 mm, which is determined by the heat source width. In this study, the plate is vertically placed, and gravity acceleration's direction follows the arrow. There are two kinds of channels in this study, as shown in Fig. 2 (b). One is a rectangle channel, which is single-layer and relatively easy to explore the geometric influence. The other is a fusiform channel, which is a double-layer and can disturb the fluid more efficiently. The inner hydraulic diameters of both channels are around 3 mm.

## 3. Numerical simulation method

It is difficult to accurately simulate a flow boiling process, especially for an object with a large scale. On the one way, the simulation methods themselves cannot include all the complex physical factors during flow boiling. On the other way, the simulation of a two-phase flow is always computationally expensive. Sometimes, we cannot mesh enough grids otherwise the simulation will cost an unacceptable long time. However, numerical simulation is still an efficient method to qualitatively compare different structures under different working conditions, different working fluid characteristics, etc., which accelerates the design.

### 3.1. Computational model

In this study, Fluent 19.0 is used as the calculation software, the three-dimensional double precision (3ddp) model is adopted, and the steady-state solver based on pressure is selected. The turbulence standard k-e model and standard wall function are selected. To improve the calculation robustness, the pressure–velocity coupled algorithm is used. The critical heat flux (CHF) model under the Euler model is selected. At the same time, the mass flow rate difference between the inlet and outlet is monitored to ensure fluctuation between them is less than 1 %.

The CHF model divides the wall heat flux $q_W$ into many partitions [52]:

$$\dot{q}_W = \left(\dot{q}_C + \dot{q}_Q + \dot{q}_E\right) f(\alpha_l) + (1 - f(\alpha_l))\dot{q}_V \tag{1}$$

where $q_C$, $q_Q$, $q_E$, $q_V$ represents the liquid convective heat flux, the quenching heat flux, the evaporative heat flux, and the vapor convective heat flux, respectively. The $f(\alpha_l)$ is a function based on the local liquid volume fraction [52].

The related main governing equations for the liquid phase (also the primary phase) are listed below.

Continuity equation [53]:

$$\frac{\partial}{\partial t}(\alpha_l \rho_l) + \nabla\left(\alpha_l \rho_l \vec{v}_l\right) = \dot{m}_{vl} - \dot{m}_{lv} \tag{2}$$

where $\alpha_l$, $\rho_l$, $v_l$ are the volume fraction, density, and velocity of the liquid phase, respectively. $m_{vl}$ and $m_{lv}$ are the mass transfer rate from the vapor phase to the liquid phase and its reverse, respectively.

Momentum equation [53]:

$$\frac{\partial}{\partial t}\left(\alpha_l \rho_l \vec{v}_l\right) + \nabla\left(\alpha_l \rho_l \vec{v}_l \vec{v}_l\right) = -\alpha_l \nabla p + \nabla \bullet \bar{\bar{\tau}}_l + \alpha_l \rho_l \vec{g} + \left(\vec{R}_{vl} + \dot{m}_{vl}\vec{v}_{vl} - \dot{m}_{lv}\vec{v}_{lv}\right) + \vec{F} \tag{3}$$

where $p$ is the pressure of both phases, $R_{vl}$ is the interaction forces between the phases and $v_{vl}$ is the velocity of the interphase. $F$ is more complex, which contains virtual mass force, lift force, wall lubrication force, and turbulent dispersion force, respectively. And $\tau_l$ in the right bracket is a stress–strain tensor [53]:

$$\bar{\bar{\tau}}_l = \alpha_l \mu_l \left(\nabla \vec{v}_l + \nabla \vec{v}_l^T\right) + \alpha_l \left(\lambda_l - \frac{2}{3}\mu_l\right) \nabla \bullet \vec{v}_l \bar{\bar{I}} \tag{4}$$

Energy equation [53]:

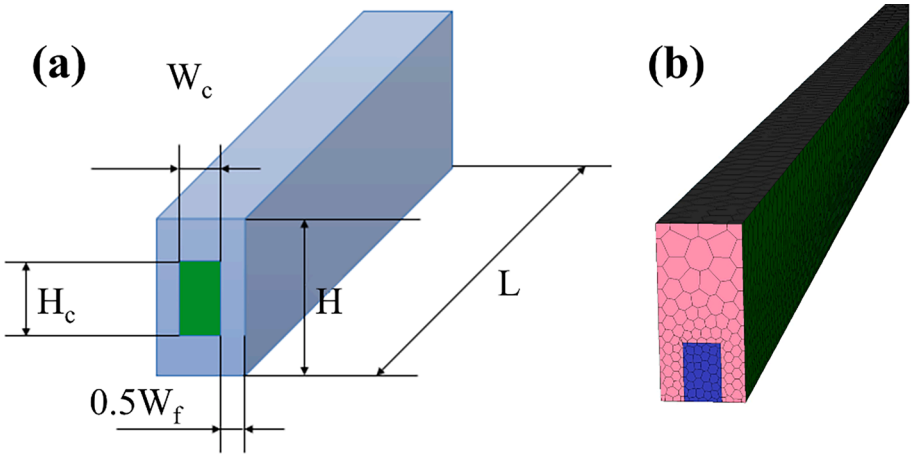


**Fig. 3.** The rectangular channel model (a) Geometric model and (b) Mesh model.

$$\frac{\partial}{\partial t}(\alpha_l\rho_l h_l) + \nabla\left(\alpha_l\rho_l \vec{u}_l h_l\right) = \alpha_l\frac{\partial p_l}{\partial t} + \bar{\bar{\tau}}_l : \nabla\vec{u}_l$$
$$-\nabla \bullet \vec{q}_l + S_l + \sum_{p=1}^{n}\left(Q_{vl} + \dot{m}_{vl}h_{vl} - \dot{m}_{lv}h_{lv}\right) \quad (5)$$

where $h_l$ and $q_l$ are the specific enthalpy and heat flux, respectively. $S_l$ is the energy source term and $Q_{vl}$ is the heat transfer from the vapor phase to the liquid phase. $h_{lv}$ and $h_{lv}$ are the enthalpies of liquid boiling to vapor and vapor condensing to liquid, respectively. Other details of the equations and some other sub-models can be found in the Fluent Theory Guide.

Besides the above calculation equations, a performance evaluation criterion (PEC) is applied here. It can evaluate the overall thermal–hydraulic performance of the rectangular channel, which is defined as [54]

$$\mathrm{PEC} = \frac{Nu/Nu_0}{(f/f_0)^{1/3}} \quad (6)$$

$$Nu = \frac{hd}{\lambda} \quad (7)$$

$$h = \frac{\dot{q}}{T_w - T_m} \quad (8)$$

$$f = \frac{\Delta P}{\left(\frac{1}{2}\rho v^2\right)(L/d)} \quad (9)$$

where $Nu$, $f$, and $h$ represent the average Nusselt number, average friction factor, and average heat transfer coefficient of the channel, and subscript 0 refers to the channel with minimum diameter.

By introducing Eqs. (7-9) into Eq. (6), replacing $T_w$ with heating-surface maximum temperature $T_{max}$, and replacing $T_m$ with phase change temperature $T_{sat}$, we can get the PEC expression:

$$\mathrm{PEC} = \frac{\left(\frac{d}{T_{max}-T_{sat}}\right)\Big/\left(\frac{d}{T_{max}-T_{sat}}\right)_0}{\left[\left(\frac{\Delta P}{v^2 d}\right)\Big/\left(\frac{\Delta P}{v^2 d}\right)_0\right]^{1/3}} \quad (10)$$

where $d$ is the hydraulic diameter of the channel, $v$ is the inlet velocity, and $\Delta P$ is the pressure drop between the inlet and outlet.

### 3.2. Geometric, grid, and boundary condition

As shown in Fig. 3, the channel width $W_C$, fin width $W_F$ and channel height $H_C$ are varied. To improve the calculation speed, a symmetric model is adopted. The fusiform channel is similar to the rectangular channel but more complex. Its final detail parameters are illustrated in Appendix. The software Fluent Meshing 19.0 is used to mesh the grid. Polyhedron mesh is adopted on the single-channel as well as the integral cold plate. Because it will have fewer cells and is easy to draw.

**Table 1**
Grid independence test.

| Grid number | $T_{max}$ /°C | Relative error | $\Delta P$ /Pa | Relative error |
|---|---|---|---|---|
| 16,384 | 80.04 | 0.10 % | 1808.7 | −1.93 % |
| 29,129 | 80.00 | 0.05 % | 1808.0 | −1.97 % |
| 70,150 | 79.99 | 0.04 % | 1830.5 | 0.75 % |
| 127,199 | 79.96 | | 1844.3 | |

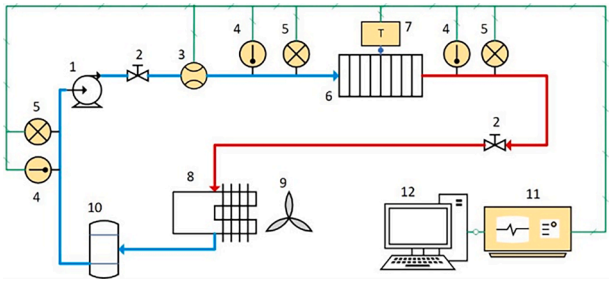


**Fig. 4.** Two-phase flow test system diagram. (1. Pump; 2. Valve; 3. Flow sensor; 4. Temperature sensor; 5. Pressure sensor; 6. Two-phase flow cold plate; 7. Multiple hot spots; 8. Air cooling condenser; 9. Fan; 10. Reservoir; 11. Data acquisition instrument; 12. Computer).

The heating surface adopts the constant heat flux boundary condition, with a heat flux $q = 7.4 \sim 11.1$ W/cm$^2$ (corresponding to 8.0 ~ 12.0 kW of an entire cold plate). The inlet and outlet are velocity and pressure boundary conditions, respectively. The bottom surface of the mesh is set as symmetry. In this section, the environmentally friendly refrigerant R1233zd(E) is selected, whose Global Warming Potential (GWP) value is 1 and ozone depletion potential (ODP) value is 0.00034 [55]. The physical properties of the liquid phase are set to change with temperature. For the vapor phase, its physical properties are the constant values at 65.5 °C saturated status, which is also the boiling point. The inlet working fluid is subcooled, whose velocity is around 0.23 m/s (corresponding to 8.0 L/min of a whole cold plate) and its temperature is 60.0 °C. The reference pressure is set as 0.454 MPa (see Table 1).

Grid independence test is carried on a rectangular channel ($W_C = 2.0$ mm, $W_F = 2.5$ mm, $H_C = 6.0$ mm) with a heat flux of 7.4 W/cm$^2$ and a velocity of 0.28 m/s. Four different numbers of grids are tested. The

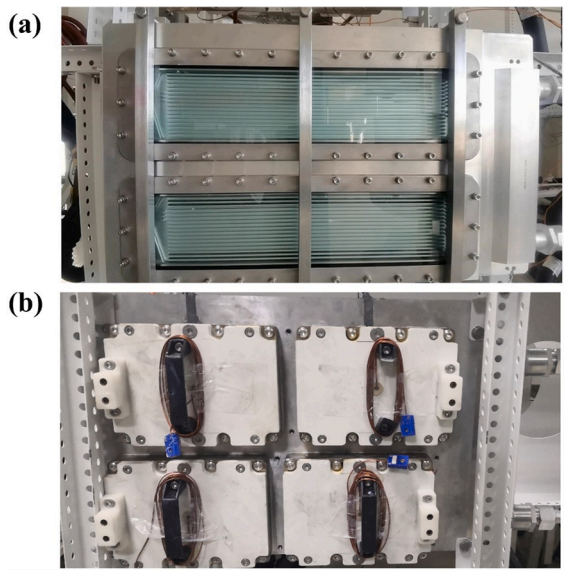


**Fig. 5.** Cold plate image. (a) Visualized plate with 4 heating blocks on one side; (b) Normal plate with 8 heating blocks on both sides.

result shows that the relative errors of $T_{max}$ and $\Delta P$ in 70,000 grids are less than 1 %, so the accordingly meshing-setting is selected for calculation.

## 4. Experiment methods

The schematic diagram of the experimental test system is shown in Fig. 4. The blue, red, and green lines represent the subcooled liquid pipeline, the two-phase fluid pipeline, and the data signal transmission line, respectively. A gear pump powers the whole system, and it works with a three-phase cyclo converter to control the flow rate. The condenser is a customized finned tube heat exchanger coupled with a small wind tunnel; its inner volume is around 11.5 L. The reservoir is made of steel, with a volume of 20 L and a relief pressure of 1.38 MPa. The temperature sensor (BANNA TE100) has a measurement range of 0 ~ 100 °C and an error of ± 0.5 °C. The pressure transmitter (BANNA PE100) has a measurement range of 0 ~ 10 bar (absolute pressure) and 0.5 % accuracy. The turbine flowmeter (BANNA FR12D) has a flow measurement range of 1 ~ 50 L/min and 1 % accuracy. All the sensors and thermal couples are linked to data acquisition equipment (YOKOGAWA GP20) with different modules. The working fluid R1233zd(E) is filled by the weighing and filling method. As shown in Fig. 5, The cold plate was made by machining and brazing with Al6061, where 8 heating blocks are arranged on both sides. Each heating block has a thermal couple in the center of the contact surface. The visualized cold plate uses tempered glass as the baffle on one side, and four heating blocks are arranged on the opposite side. Because CNC machining for a whole tempered glass is difficult, two layers of tempered glass are used. The inner glass is embedded, which contacts the channel. And the outer is used to compress the seal ring. There is a 0.2 mm gap between the two glasses to avoid local stress concentration, which has an inevitable disadvantage on the visualized image.

## 5. Results and discussion

### 5.1. Design by simulation

The design follows the principle from the single channel to the whole cold plate. As shown in Fig. 5(a), the increase of $W_F$ and the decrease of $H_C$ will lead to a decrease in the heat exchange area, causing the increase of $T_{max}$, which has an approximately linear correlation. Besides, it shows

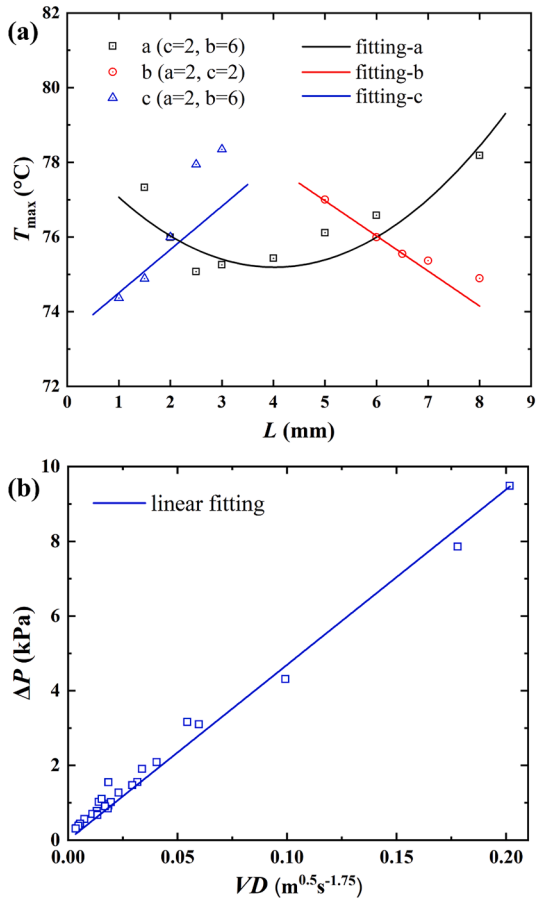


**Fig. 6.** (a) Relationship between parameters' value and temperature value; (b) Relationship between combined parameter's value and pressure drop.

that $T_{max}$ first decreases and then increases with the channel width $W_C$, while the distribution is approximately a second power function. If we use the value of $W_C$, $H_C$, and $W_F$ in millimeter units as $a$, $b$ and $c$, the mathematic relationship of the parameters with the temperature's value will be Eq. (11), whose $R^2 = 0.893$:

$$T = 0.205a^2 - 1.649a - 0.940b + 1.276c + 81.596(^{\circ}\mathrm{C}) \tag{11}$$

The velocity of the working fluid is very high so it is turbulent. Compared with the pressure drop calculation formula in the fully developed turbulence section, we multiply $V^{1.75}$ and $d^{-1.25}$ as the combined parameter $VD$ to study its influence on the pressure drop $\Delta P$. Similarly, the linear function of the fitting is Eq. (12), whose $R^2 = 0.992$:

$$\Delta P = 44618 \times \left[\frac{269(a+c)}{360ab}\right]^{1.75}\left(\frac{2ab}{a+b}\right)^{-1.25} + 230.59(\mathrm{Pa}) \tag{12}$$

The two fitting functions are shown in Fig. 6.

By introducing Eq. (11) and Eq. (12) into Eq. (10), we can obtain the expression of PEC about the three geometric parameters. Using constrained minimization for multivariate nonlinear functions (constraints condition: 2.5 mm ≤ $a$ ≤ 3.5 mm, 3 mm ≤ $b$ ≤ 6.5 mm, 2.5 mm ≤ $c$ ≤ 4 mm), we can get the geometric parameters corresponding to the maximum PEC as $a$ = 2.5 mm, $b$ = 6.5 mm, and $c$ = 4 mm by using global search in MATLAB. Because the gear pump has high heads, to further reduce $T_{max}$ and consider the mechanical processing convenient, the final dimensions are maintained as $a$ = 2.5 mm, $b$ = 6.5 mm, and $c$ = 2.5 mm.

The better flow uniformity, the better temperature control. The whole cold plate design mainly concerns the flow distribution structure. Fig. 7 shows the simulation comparison before and after a structural

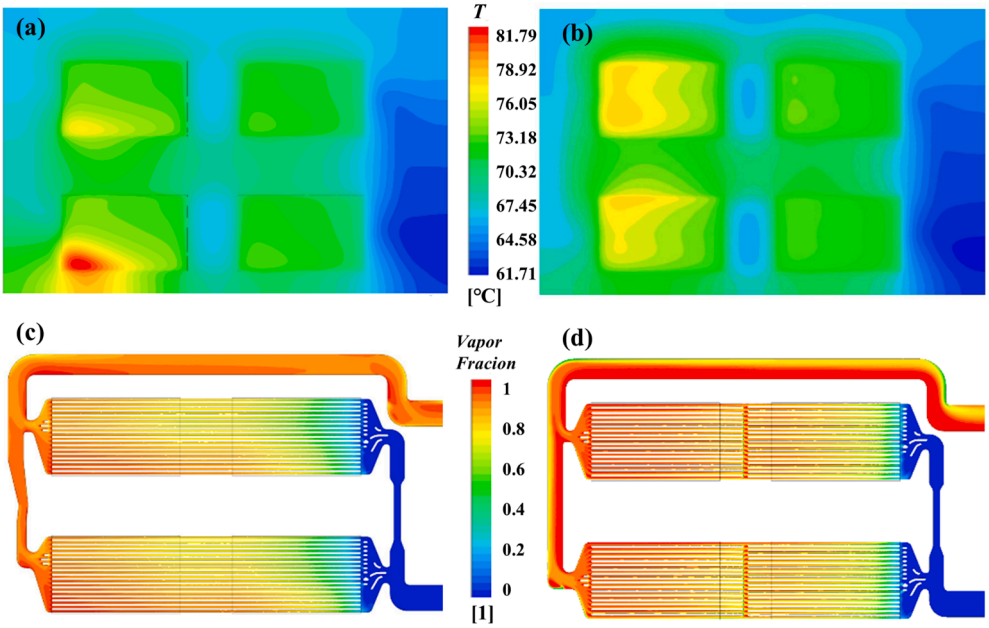


**Fig. 7.** Simulation results with different flow distribution structures (a) Temperature contour before improvement; (b) Improved temperature contour; (c) Vapor fraction contour before improvement; (d) Improved vapor fraction contour.

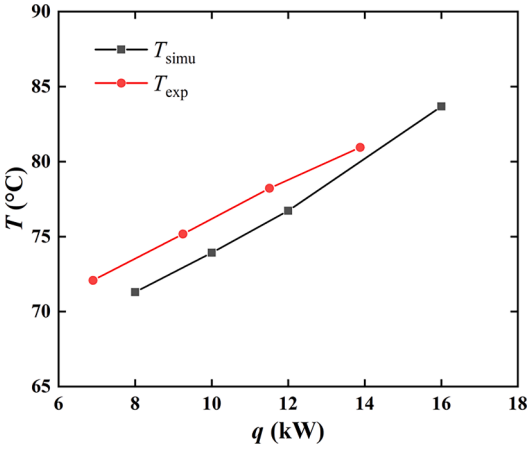


**Fig. 8.** The temperature comparison between the experiment and CFD simulation.

improvement. Their inside channel structures are shown in Fig. 7 (c-d). The structures of the upper half branch and lower half branch are not completely the same, aiming at balancing the flow resistance. It can be found that there is an overheating zone in the lower branch before improvement. The distribution of vapor fraction among branches is uneven, implying the unreasonable distribution of fluid. In this regard, the outlet channel of the lower half branch is widened, and a staggered structure is added. After this adjustment, the flow uniformity is significantly improved. Correspondingly, the temperature distribution becomes more uniform. Therefore, simulation can be used as the optimization basis for design to uniform the flow distribution and eliminate local overheating areas.

### 5.2. Comparison of experiment and simulation

The simulation needs to be tested by experiments. As shown in Fig. 8, the flow rate of the cold plate with a fusiform channel maintains at 8 L/min, while its heating power $q$ varies. The result shows that the experimental temperature $T_{exp}$ is always higher than the simulation

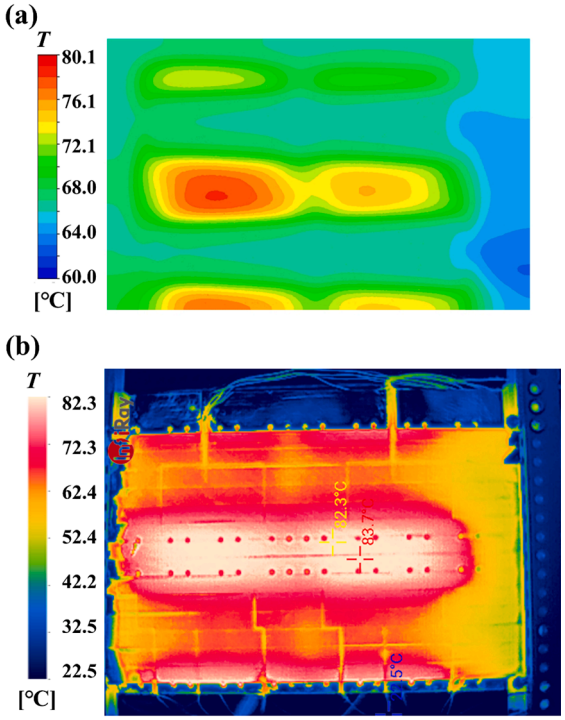


**Fig. 9.** The temperature distribution comparison between the experiment and CFD simulation. (a) CFD simulation temperature contour; (b) Experimental infrared thermogram.

temperature $T_{simu}$. On one way, the inner pressure of the cold plate is uncertain, so we set a constant value for the boiling point in the simulation. However, the experimental boiling point is higher and decreases along the flow path, this will cause some calculation differences. On the other way, as the heating power increase from 6.9 kW to 13.88 kW, the closed system will have a bigger vapor fraction with larger average specific gravity. So the absolute pressure will be higher, and the pressure near the inlet of the plate increase from 4.588 bar to 4.951 bar. And the

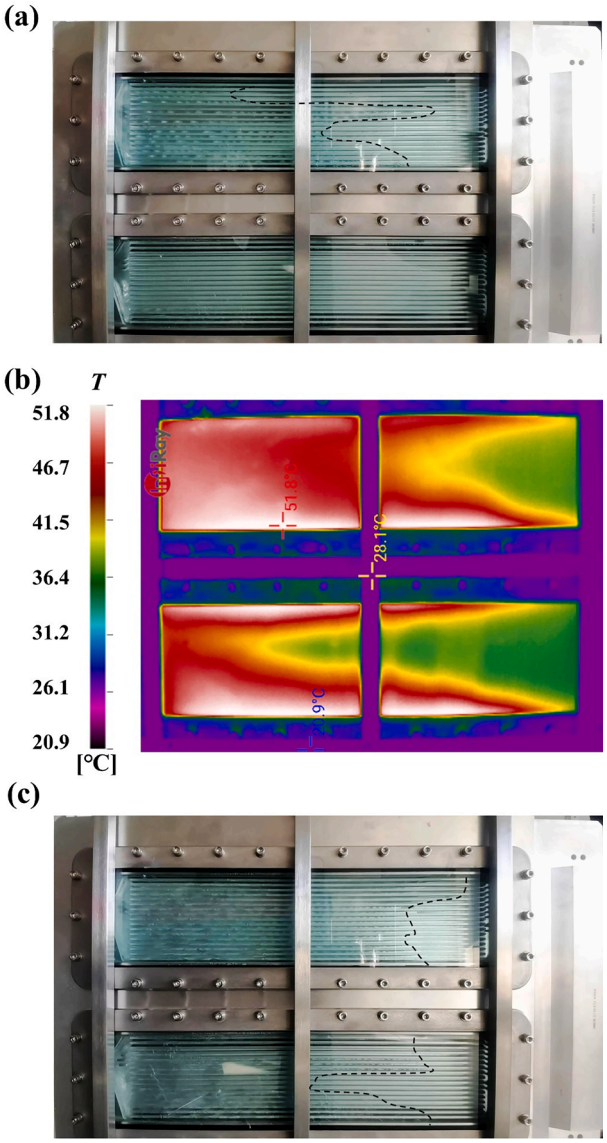


**Fig. 10.** Experimental images of a cold plate (a) Flowing image with low heating power; (b) Thermal image with low heating power; (c) Flowing image with medium heating power.

relevant saturation temperature of the working fluid is 65.82 °C to 68.84 °C, they are all higher than the setup boiling point of 65.5 °C. The higher the boiling point, the higher the supercooled degree. So the simulated temperature of the cold plate is lower than the experiment.

To maintain the computation speed, the grids number of the whole cold plate is about 3 million. The calculations are carried out using constant physical properties for convergence. These factors produce some calculation errors. The boiling point is relative to the inner absolute pressure of the plate. And the pressure drop of the plate is much smaller relative to the absolute pressure of the working fluid. So utilizing variable boiling points will not affect the results a lot. Besides, since the boiling point is difficult to know in advance, the CFD simulations are more like qualitative references to guide the design. As shown in Fig. 9, the temperature distribution in the simulation is similar to the experiment. The edge temperature of the heating block area is high because there is no flow channel under the bolt connection place. However, it is not similar to Fig. 7 at all. Because in the experiments, the heating block is a thick copper block, heat will be conducted to its edge area with high efficiency. The real electric device will generate heat evenly, mainly in the center. So the simulation heating boundary area in Fig. 7 is smaller

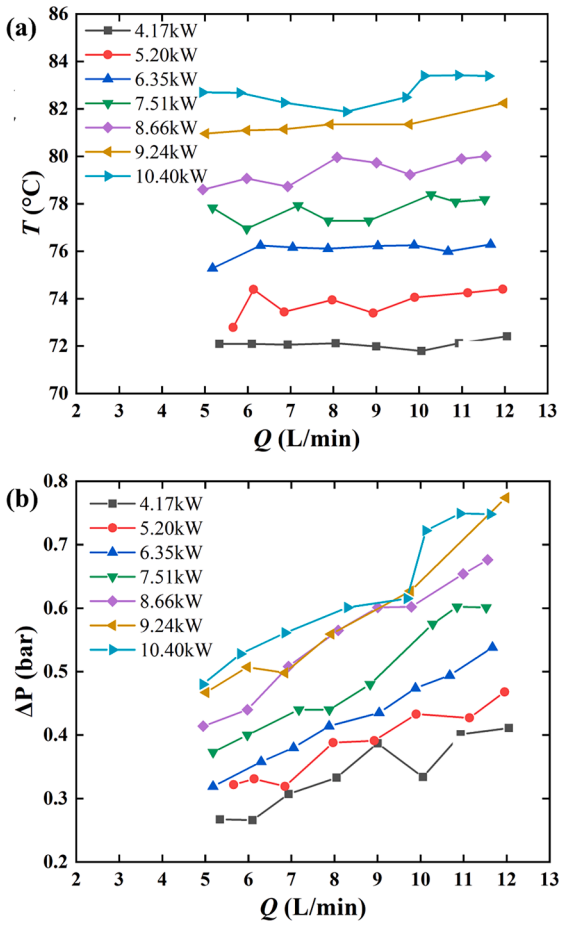


**Fig. 11.** Experimental results of the cold plate under variable working conditions. (a) Temperature to flow rate relationship under variable heat load; (b) Pressure drop to flow rate relationship under variable heat load.

than in Fig. 9. And the temperature in the center line with a real electric device will be cooler. Besides, even in the worse assumption shown in Fig. 9, because there is no important electric device placed in the center, the high temperature and thermal stress won't affect the system. Additionally, because the boiling point drops throughout the flow channel, the negative effects of a rise in working fluid temperature are lessened. It appears the experimental temperature distributes more evenly along the flow path than the simulation. To be more specific, although the working fluid's temperature increases with the flow, making it is more difficult to absorb heat by using sensible heat. The decreased $T_{sat}$ makes it easier to evaporate and use its latent heat. The difference in heat exchange capability of working fluid is weakened along the flow path in experiments.

### 5.3. Flow and heat transfer characteristics

The flow boiling phenomenon is much more complex than the single-phase flow. Some experience in single-phase water cold plate design might be unsuitable. It is essential to know the basic flow and heat transfer characteristics of the two-phase cold plate. The following are the experimental results of the cold plate with rectangular channels and refrigerant R1233zd(E).

#### 5.3.1. Flow analysis

This section mainly analyzes the flow characteristics of the cold plate by visualizing the boiling phenomenon. If the heating power is beyond 8 kW, the flow boiling will become too violent and too fast, and few flow details can be seen. As shown in Fig. 10 (a-b), the low heating power of

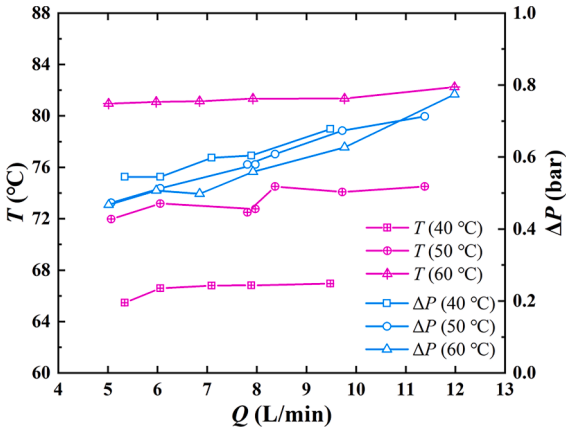


**Fig. 12.** Experimental results of cold plate temperature and pressure drop changes with flow rate ($q$ = 9.24 kW).

1.84 kW and a flow rate of 8.38 L/min are chosen in the experiment, where the refrigerant is R1233zd(E). The black dotted line shows where the birthplace of bubbles. The upper half branch has a large slug flow area, indicating it contains fewer working fluids than the lower branch. Accordingly, the high-temperature area of the upper branch is bigger. Similar to Fig. 9 (b), it can be found that the maximum temperature appears at the edge of both branches, where no flow channel exists inside. But the real heat sources will maintain in the center, so the real performance will be significantly improved.

In Fig. 10 (c), the low heating power is 4.16 kW and its flow rate is 8.93 L/min. With the increase of heating power, the region where the phase change biases to the inlet and the difference in bubble region between the upper and lower branches decreases. Because the proportion of pressure drop in the channel region to the total pressure drop increases under a high heat load. The difference in flow resistance between the upper and lower branches decreases correspondingly.

### 5.3.2. Heat transfer analysis

This section mainly analyzes the experiment results of a cold plate with rectangular channels under variable working conditions. The inlet temperature $T_{in}$ of R1233zd(E) is 60 °C. Because the cold plate will not always work under a high heat load, it is necessary to study the performance under a lower heat load. In Fig. 11 (a), there is an abnormal phenomenon that the cold plate temperature $T$ in the test will slightly increase with the flow rate. Because when the flow rate increase, the inlet and outlet pressure of the cold plate will also increase in the closed system. Correspondingly, the boiling point and the supercooled degree of the working fluid increase, making boiling more difficult to happen. Through the temperature lines, it can be found that the trend of temperature and flow rate is approximately parallel in all situations. The temperature increases by about 2 °C for every 1 kW increase in the heating power. The thermal resistance of the cold plate is defined as Eq. (13).

$$r_{plate} = \frac{T - T_{in}}{q} \tag{13}$$

The $r_{plate}$ gradually decreases from $3.3 \times 10^{-3}$ K/W to $2.6 \times 10^{-3}$ K/W corresponding to the heating power increase from 4.17 kW to 10.40 kW. It indicates that the flow boiling becomes more intense with the increase of heating power. In Fig. 11 (b), the pressure drops change with the flow rate and the heating power approximately linearly rather than quadratically. Because the vapor accounts for more at a low flow rate than at a high flow rate, resulting in little difference in the volume flow rate near the outlet region. The flow velocity changes approximately linearly within the existing parameter range, the same as the pressure drop.

The actual ambient conditions may be cooler, so it is also necessary to experiment with cooler working fluid. As shown in Fig. 12, the change of $T_{in}$ does not affect the trend that the cold plate temperature $T$ slightly

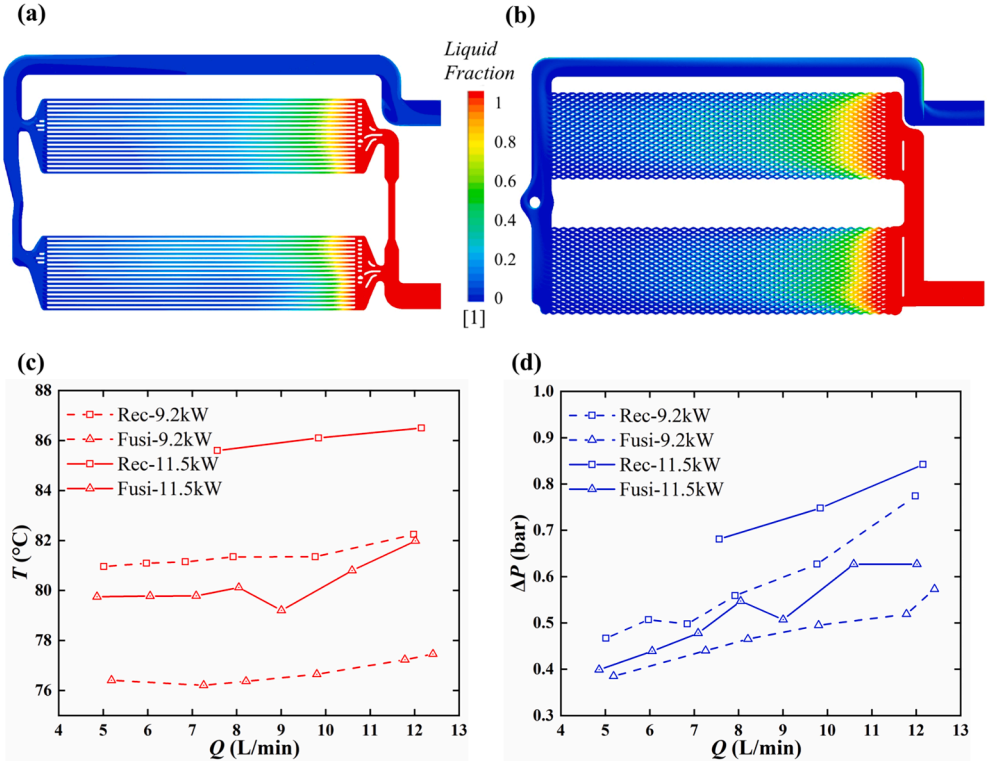


**Fig. 13.** The comparison of the different channel structures. Simulation results of liquid fraction in cold plates with (a) rectangular channels and (b) fusiform channels; (c) Experimental temperature, and (d) Experimental pressure drop results of cold plates with different channel structures.

**Table 2**
Different refrigerants properties and numerical simulation.

| Properties | Units | Types | | | | |
|---|---|---|---|---|---|---|
| | | R134a | R1234ze(E) | R236fa | R1233zd(E) | HFE-7100 |
| Latent heat [a] | J/kg | 132,060 | 129,290 | 118,250 | 167,740 | 109,200 |
| Liquid specific heat [a] | J/(kg·K) | 1730.5 | 1604.0 | 1402.9 | 1296.4 | 1255.0 |
| Pressure [a] | MPa | 1.9116 | 1.4532 | 0.8804 | 0.4541 | 0.1160 |
| Gas density [a] | kg/m$^3$ | 101.81 | 81.17 | 60.31 | 24.01 | 11.08 |
| Liquid density [a] | kg/m$^3$ | 1022.8 | 1007.8 | 1206.7 | 1157.4 | 1360.3 |
| Merit number, $\times 10^9$ | kg$^2$·m/s$^6$ | 5.50 | 5.37 | 4.51 | 6.39 | 1.26 |
| d$P$/d$T$ [a] | MPa/K | 0.0438 | 0.0337 | 0.0221 | 0.0121 | 0.0037 |
| GWP$_{100}$ | 1 | 1430 | 6 | 9810 | 1 | 297 |
| ODP | 1 | 0 | 0 | 0 | 0.00034 | 0 |
| Pressure drop [b] | Pa | 440.8 | 547.0 | 839.0 | 1019.9 | 3438.9 |
| Maximum surface temperature [b] | ℃ | 70.64 | 71.30 | 72.63 | 74.96 | 86.23 |

[a] obtained at the saturation temperature of 65.5 °C.
[b] CFD simulation results of one rectangular channel (6.5 mm × 2.5 mm × 2.5 mm).

increases with flow rate $Q$. However, it can be found that the thermal resistance decreases with $T_{in}$. Because the vapor–liquid density ratio of R1233zd(E) decreases at a higher temperature, its flow uniformity and heat transfer performance are better. So, we may overestimate the cold plate temperature if we use the one with lower $T_{in}$ to forecast by simply adding the difference in $T_{in}$. For the same system, if we want to examine another working fluid with high saturation pressure at the same temperature. The pressure tolerance of the system components may not be enough. So experimenting at the same high temperature is not safe. However, we can experiment with a lower temperature corresponding to a lower safe pressure. In this way, we can estimate the cold plate's real temperature performance with a conservative value. This will benefit the comparison of different working fluids with less cost.

### 5.4. Comparison of channel type

Ideal cold plate has a high heat transfer coefficient, a small flow resistance, and well flow uniformity. So, its surface temperature can maintain a uniform low value. Although adding an extra flow distribution structure can force the fluid to flow as we wish, the pressure increases inevitably with no other benefits. So, using a staggered channel may be a better way. Because it not only enhances the flow uniformity between parallel channels but also increases the heat transfer coefficient.

$$q = h_{avg} \cdot A \cdot \Delta T = h_{avg} \cdot A \cdot \overline{\sum (T - T_{sat})} \tag{14}$$

Eq. (14) qualitative reveals the relationship between heating power $q$ and cold plate temperature $T$. According to our visual experiment, the working fluid will evaporate violently from the inlet channel area under high heat flux. Because the flow will be boiling in most area under the current boundary condition, we used the $T_{sat}$ in the equation. There are three methods to decrease $T$. Firstly, we can increase the overall average heat transfer coefficient $h_{avg}$ by reducing the boundary layer. If the flow rate is sufficient, the flow boiling is always violent and highly efficient for a heat flux of 10 W/cm$^2$ level. In this case, improving the flow uniformity may be more important. Secondly, we can increase the heat exchange area by applying more complex and compact channels. However, the pressure drop rise must be taken into account. The boiling point will change a lot in too dense structure which infects temperature uniformity. Thirdly, increasing the flow cross-section area will decrease the pressure drop and $T_{sat}$. However, it is very limited. Sometimes, a different kind of working fluid may be more useful.

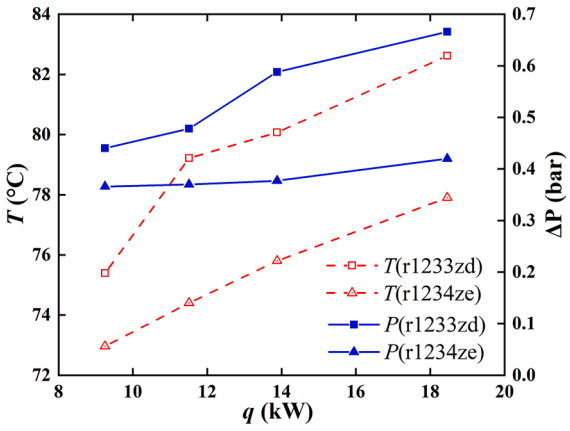


**Fig. 14.** Experimental average surface temperature and pressure drop results of R1233zd(E) and R1234ze(E) in the fusiform cold plate with a flow rate around 7 L/min.

As shown in Fig. 13, the fusiform channel is denser than the rectangular channel. Their heat exchange areas are 0.371 m$^2$ and 0.235 m$^2$, respectively. To reduce the thermal resistance and increase the heat exchange area, the fusiform channel is double-layer (the $H_C$ is 3.5 mm for each layer). So the minimum distance between the inner channel and the cold plate surface changes from 5.75 mm to 3.5 mm, which can still tolerate the pressure of R1233zd(E) and R1234ze(E). Referring to the above experimental results in Fig. 9, the total width of the channel was also increased a little to lower the edge temperature. Because of the staggered fusiform structure, its flow uniformity will be better, which is consistent with the simulation result. And the flow boundary layer should be thinner in the impact face as well, which further increases the heat transfer rate on the inner surface of the channel. So, the experimental temperature of the fusiform cold plate is almost 5 °C lower than the rectangular. Besides, because the cross-section area of the fusiform one increases, the pressure drop even decreases by 0.1 ~ 0.2 bar, which further decreases the $T_{sat}$ and enhances the boiling process. Overall, the double-layer cold plate with a fusiform channel has a great advantage over the single-layer cold plate with rectangular channels on every field except pressure tolerance.

### 5.5. Comparison of working fluid type

There are abundant choices for working fluid. A suitable working fluid has a decisive influence on the system's performance which is well worth exploring. In a practical design job, the thermal engineer ought to choose the proper working fluid according to the working condition and estimate its flow rate according to the heat load. It is easy to estimate and compare the heat transfer performance of different working fluids, which is determined by their physical properties. However, we also need to consider environmental requirements (such as GWP and ODP), long-term safety, and so on.

In Table 2, a series of refrigerant properties are listed [55]. Except for normal properties, a merit number ($=\rho_v \cdot h_{lv}^2 \cdot \sigma$) and d$P$/d$T$ are listed [56]. In general, the higher the merit number, the better performance on

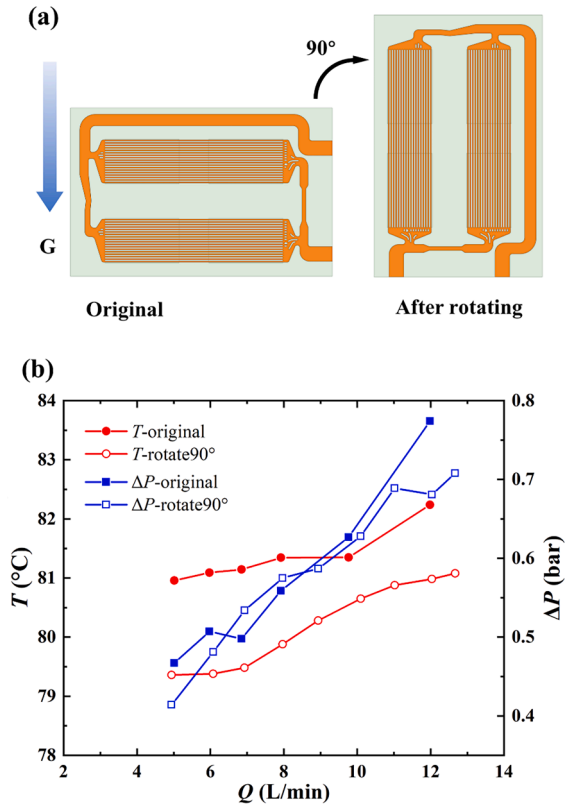


**Fig. 15.** Performance comparison of the cold plate in the different gravity orientations. (a) Schematic diagram before and after rotation; (b) Temperature and pressure drop changes with flow rate.

vapor pressure drop. And the higher the value of d$P$/d$T$, the lower the thermal resistance of the plate. So R134a should have the best temperature performance among the listed types. Because the comparison of different refrigerants should be carried out before the structure optimization. Numerical simulations are carried out for each refrigerant using the same single rectangular channel for high calculation speed. During simulation, the working fluid has an inlet temperature of 60 °C and a boiling point of 65.5 °C. Their flow rate is calculated by making the output steam quality equal to 0.26. The simulation results show that the higher d$P$/d$T$, the better the performance. However, the relative pressure is high and undesired for the system's long-term safety, especially in a sustainable vibration environment. The thickness of the cold plate may have to increase accordingly as well.

Because environmentally friendly refrigerants are required in more and more places, the refrigerants R1233zd(E) and R1234ze(E) are chosen for experiments. As shown in Fig. 14, the cold plate temperature with R1234ze(E) is 5 °C lower than the same cold plate using R1233zd (E), which is consistence with the simulation trend. Its pressure drop is also much smaller than R1233zd(E), especially in high heating power conditions. Because the difference in outlet volume flow rate is much larger under high heating power. The more the velocity difference, the more the pressure drop difference. What's more, with less pressure drop within the cold plate, the boiling point will be lower and enhance the heat transfer performance. Unless we value the system pressure bear a lot, using R1234ze(E) will result in better performance.

### 5.6. Flow uniformity improvement

Obviously, by changing the channel structure from rectangular to fusiform, its flow uniformity will be improved. However, the final heat transfer enhancement is affected by a lot of reasons. The single effect of flow uniformity still needs to study. In previous Fig. 10, the cold plate

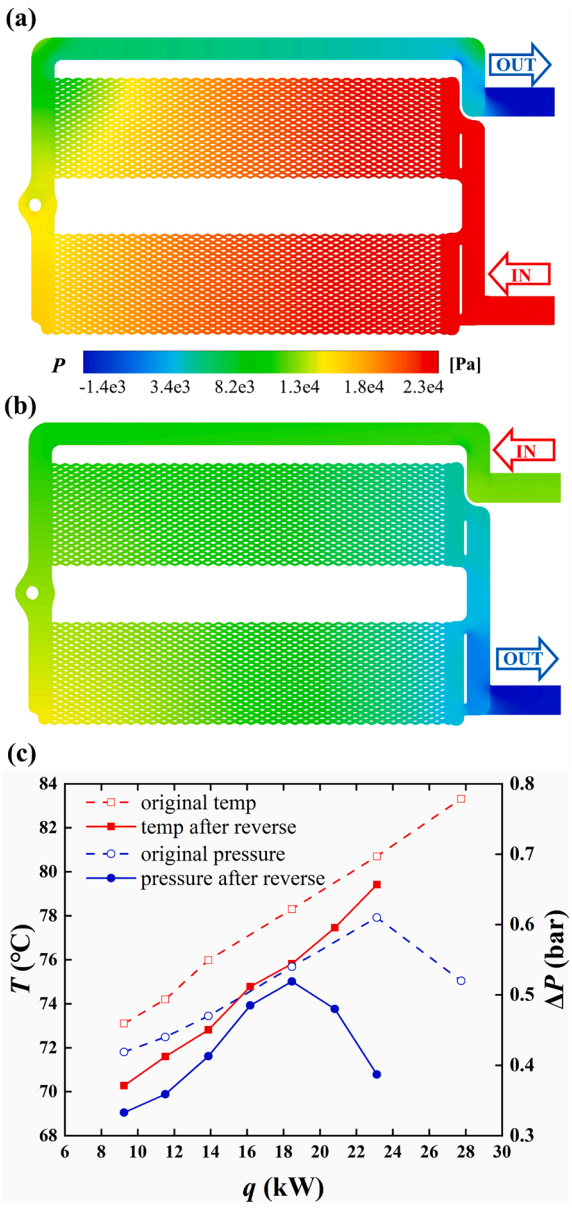


**Fig. 16.** Performance comparison of the cold plate in different ways of in and out. (a) The simulation pressure contour of a cold plate with down-in and up-out; (b) The simulation pressure contour of a cold plate with up-in and down-out; (c) The experimental comparison of temperature and pressure drop performance to various heat loads after reversing the inlet and outlet.

with rectangular channels has a lower flow rate at the upper branch, where gravity has a bad influence. Besides, the flow rate in parallel channels of neither branch is very uniform. So, we change the gravity orientation by rotating the cold plate to improve the flow uniformity conveniently.

In Fig. 15 (a), G is the symbol of gravity acceleration. After rotating 90°, the working fluid changes from left in and right out to up in and down out. The curves in Fig. 15 (b) show that $T$ decreases about 1.5 °C and $\Delta P$ changes little after rotation, indicating a great impact of gravity on the flow distribution. Because the heating power is about 9 kW, the flow boiling is very violent in the two-phase region. Through the former visualized experiment, the flow is annular flow or mist flow with a very high speed. The influence of flow pattern change under different gravity orientations should not be very pronounced. After rotation, the branches have less difference in flow resistance, so as do the parallel channels. The flow uniformity will be improved, avoiding the high temperature in the

less-flow-rate region. Overall, the flow uniformity improvement achieved by rotation alone can benefit temperature control to some degree.

### 5.7. Pressure drop improvement

Inspired by numerical simulation, the influence of pressure drop alone is studied on the fusiform cold plate. As shown in Fig. 16 (a), the simulation results show a large pressure drop existing in the bending channel near the outlet. Because the working fluid at the outlet is a very fast two-phase flow (15 m/s or more). There will be large momentum loss and local pressure drop when it passes through multiple right-angle turns. Therefore, it is considered to change the position of the inlet and outlet. Fig. 16 (b) shows the pressure drop decreased after the exchange. Because the multiple right-angle turns are on the inlet liquid side with a small flow rate.

Supported by the simulation results, a comparison experiment is done later. Fig. 16 (c) shows the experimental performance of the cold plate to heat load before and after the reverse. Here, the working fluid is R1234ze(E) with a flow rate of 9.0 ± 0.5 L/min. It can be seen that the performance of the cold plate improves significantly after the inversion of the import and export, and the temperature can drop by about 3 °C. But the pressure drop does not decrease as much as in the simulation. Because there are some joints and pipes between the pressure sensor and the cold plate. The experimental pressure drop contains more parts except for the cold plate, so it is higher than the simulation. And the other parts of the pressure drop will not change apparently if we only exchange the inlet and outlet of the cold plate. So, the total pressure drop decreases a little after the exchange of the inlet and outlet. It is strange that the pressure drop decrease at high loads. However, this phenomenon rarely happens if we put all the experiments into account. One possible explanation is the flow instability of the pumped two-phase flow system, especially with high heating power. It is beyond the scope of this study and may need more careful research. Anyway, if there are many bends in the flow path, they should be placed on the liquid inlet side to improve the performance of the cold plate.

## 6. Conclusion

In this study, the flow and heat transfer performance of the mini-channel two-phase cold plate with high heating power is studied by simulation and experiments. Rectangular channels and fusiform channels are applied. The best cold plate in our design, which uses R1234ze (E) with a temperature of 60 °C and a flow rate of 9 L/min, can maintain its surface temperature below 80 °C and its pressure drop below 0.6 bar under 20 kW heat load. The following conclusions can be summarized from the simulation and experimental results.

(1) The numerical simulation can help to select the channel parameters and design the flow distribution structure. There are some calculation errors due to the model's and grids' limitations, but the relative distributions of parameters are in good agreement with the experiment, which can still guide the design.
(2) The abnormal phenomenon that the temperature increases with the flow rate in the experiment is caused by the positive correlation coupling between the boiling point and flow rate. With the increase of heating power, due to the increased account of pressure drop in the channel part, the flow resistance difference between branches is weakened, leading to better flow uniformity.
(3) Through simulations and experiments, the double-layer cold plate with fusiform channels has a great advantage over the single-layer cold plate with rectangular channels on every field except pressure tolerance. The heat exchange area and flow uniformity are very important factors for the two-phase cold plate design.
(4) Using R1234ze(E) as the working fluid, the temperature and pressure drop performance of the system is better than using R1233zd(E). Unless we value the system pressure bear a lot, using R1234ze(E) at a relatively high saturated temperature will be better.
(5) The flow uniformity and pressure drop of the two-phase cold plate can influence its performance. If possible, try to avoid placing the parallel channels perpendicular to the gravity direction. And if there are many bends inside the cold plate, they should be placed on the liquid inlet side.

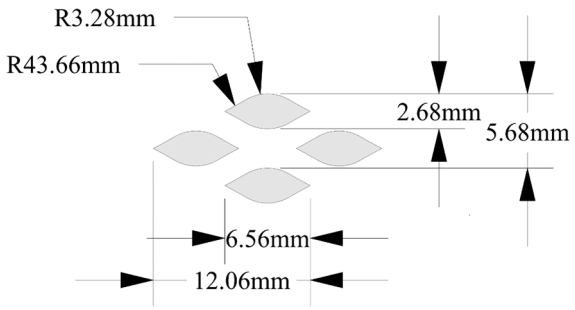


**Fig. A1.** Geometry details of the fusiform channel.

## Declaration of Competing Interest

The authors declare that they have no known competing financial interests or personal relationships that could have appeared to influence the work reported in this paper.

## Data availability

the data has been involved in the manuscript

## Acknowledgments

The research was supported by the National Natural Science Foundation of China (No.52076088) and the Foundation of State Key Laboratory of Coal Combustion (FSKLCCA2007).

## Appendix

See Fig. A1.

## References

[1] Z. Deng, J. Shen, W. Dai, K. Li, Q. Song, W. Gong, X. Dong, M. Gong, Experimental study on cooling of high-power laser diode arrays using hybrid microchannel and slot jet array heat sink, Appl. Therm. Eng. 162 (2019), 114242.
[2] H. Tan, K. Zong, P. Du, Temperature uniformity in convective leaf vein-shaped fluid microchannels for phased array antenna cooling, Int. J. Therm. Sci. 150 (2020), 106224.
[3] M. Pan, M. Hu, H ., Wang, Study of the performance of an integrated liquid cooling heat sink for high-power IGBTs, Appl. Therm. Eng. 190 (2021), 116827.
[4] X. Lin, S. Mo, B. Mo, L. Jia, Y. Chen, Z. Cheng, Thermal management of high-power LED based on thermoelectric cooler and nanofluid-cooled microchannel heat sink, Appl. Therm. Eng. 172 (2020), 115165.
[5] E. Baker, Liquid cooling of microelectronic devices by free and forced convection, Microelectron. Reliab. 11 (2) (1972) 213–222.
[6] B.P. Benam, A.K. Sadaghiani, V. Yagci, M. Parlak, K. Sefiane, A. Kosar, Review on high heat flux flow boiling of refrigerants and water for electronics cooling, Int. J. Heat Mass Transfer. 180 (2021), 121787.
[7] M.B. Bowers, I. Mudawar, High flux boiling in low flow rate, low pressure drop mini-channel and micro-channel heat sinks, Int. J. Heat Mass Transfer. 37 (2) (1994) 321–332.
[8] S.S. Mehendale, A.M. Jacobi, R.K. Shah, Fluid Flow and Heat Transfer at Micro- and Meso-Scales With Application to Heat Exchanger Design, Appl. Mech. Rev. 53 (2000) 175–193.
[9] S.G. Kandlikar, Two-Phase Flow Patterns, Pressure Drop, and Heat Transfer during Boiling in Minichannel Flow Passages of Compact Evaporators, Heat Transfer Eng. 23 (1) (2002) 5–23.
[10] P.A. Kew, K. Cornwell, Correlations for the prediction of boiling heat transfer in small-diameter channels, Appl. Therm. Eng. 17 (8-10) (1997) 705–715.

[11] P. Cheng, H.Y. Wu, Mesoscale and Microscale Phase-Change Heat Transfer, Advances in Heat Transfer, Elsevier (2006) 461–563.
[12] M.S. Patil, J.-H. Seo, S. Panchal, S.-W. Jee, M.-Y. Lee, Investigation on thermal performance of water-cooled Li-ion pouch cell and pack at high discharge rate with U-turn type microchannel cold plate, Int. J. Heat Mass Transfer. 155 (2020), 119728.
[13] T. Wen, H. Zhan, L. Lu, D. Zhang, Experimental investigation and development of new correlation for flow boiling heat transfer in mini-channel, Int. J. Therm. Sci. 129 (2018) 209–217.
[14] K. Strak, M. Piasecka, The applicability of heat transfer correlations to flows in minichannels and new correlation for subcooled flow boiling, Int. J. Heat Mass Transfer. 158 (2020), 119933.
[15] K. Kurose, W. Noboritate, S. Sakai, K. Miyata, Y. Hamamoto, An experimental study on flow boiling heat transfer of R410A in parallel two mini-channels heated unequally by high-temperature fluid, Appl. Therm. Eng. 178 (2020), 115669.
[16] Y. Kubo, S. Yamada, H. Murakawa, H. Asano, Correlation between pressure loss and heat transfer coefficient in boiling flows in printed circuit heat exchangers with semicircular and circular mini-channels, Appl. Therm. Eng. 204 (2022), 117963.
[17] G. Zhu, T. Wen, D. Zhang, Machine learning based approach for the prediction of flow boiling/condensation heat transfer performance in mini channels with serrated fins, Int. J. Heat Mass Transfer. 166 (2021), 120783.
[18] J. Li, H. Hu, Y. Zhang, Experimental investigation and correlation development for two-phase pressure drop characteristics of flow boiling in offset strip fin channels, Int. J. Therm. Sci. 160 (2021), 106693.
[19] B. Markal, A. Candan, O. Aydin, Flow boiling characteristics in a novel minichannel with a step on each corner, Exp. Heat Transfer. 33 (1) (2020) 1–17.
[20] A.V. Belyaev, A.N. Varava, A.V. Dedov, A.T. Komov, Critical heat flux at flow boiling of refrigerants in minichannels at high reduced pressure, Int. J. Heat Mass Transfer. 122 (2018) 732–739.
[21] D. Hellenschmidt, P. Petagna, Effects of saturation temperature on the boiling properties of carbon dioxide in small diameter pipes at low vapour quality: Heat transfer coefficient, Int. J. Heat Mass Transfer. 172 (2021) 121094.
[22] T. Layssac, S. Lips, R. Revellin, Effect of inclination on heat transfer coefficient during flow boiling in a mini-channel, Int. J. Heat Mass Transfer. 132 (2019) 508–518.
[23] Y. Kuang, W. Wang, J. Miao, X. Yu, H. Zhang, Pressure drop instability analysis in mini-channel evaporators under different magnitudes of gravity, Int. J. Therm. Sci. 147 (2020), 105952.
[24] G. Li, X. Fang, Z. Luo, Y. Qin, Flow boiling characteristics of water in a horizontal tube under hypergravity environment, Journal of Aerospace Power 37 (2022) 46–54.
[25] M. Azzolin, S. Bortolin, Condensation and flow boiling heat transfer of a HFO/HFC binary mixture inside a minichannel, Int. J. Therm. Sci. 159 (2021), 106638.
[26] C.-H. Kim, N.-H. Kim, Evaporation heat transfer and pressure drop of low GWP R-404A alternative refrigerants in a multiport tube, Int. J. Heat Mass Transfer. 184 (2022), 122386.
[27] S.K. Gupta, R.D. Misra, An experimental investigation on flow boiling heat transfer enhancement using Cu-TiO2 nanocomposite coating on copper substrate, Exp. Therm Fluid Sci. 98 (2018) 406–419.
[28] M. Aravinthan, S. Sarkar, P. Dhar, S.K. Das, A.R. Balakrishnan, Flow Boiling Heat Transfer Characteristics in Minitubes With and Without Hydrophobicity Coating, Heat Transfer Eng. 41 (3) (2020) 288–301.
[29] B. He, X. Luo, F. Yu, J. Zhou, J. Zhang, Flow boiling characteristics in bi-porous minichannel heat sink sintered with copper woven tape, Int. J. Heat Mass Transfer. 158 (2020), 119988.
[30] H.-W. Li, Y.-C. Wang, C.-H. Du, W.-P. Hong, Analysis of flow pattern change in horizontal mini-channel under electric field force, Int. Commun. Heat Mass Transfer. 121 (2021), 105081.
[31] J.D. de Oliveira, J.B. Copetti, M.L. Sperb Indrusiak, R.R. de Souza, R. Lima, On the nature of flow patterns and pressure drop fluctuations during flow boiling, Int. J. Multiphase Flow. 144 (2021), 103793.
[32] G. Rafalko, R. Mosdorf, G. Gorski, Two-phase flow pattern identification in minichannels using image correlation analysis, Int. Commun. Heat Mass Transfer. 113 (2020), 104508.
[33] A. Chen, T.F. Lin, H.M. Ali, W.-M. Yan, Experimental study on bubble characteristics of time periodic subcooled flow boiling in annular ducts due to wall heat flux oscillation, Int. J. Heat Mass Transfer. 157 (2020), 119974.
[34] H. Grzybowski, R. Mosdorf, Dynamics of pressure drop oscillations during flow boiling inside minichannel, Int. Commun. Heat Mass Transfer. 95 (2018) 25–32.
[35] S. Hong, C. Dang, E. Hihara, H. Sakamoto, M. Wada, Improved two-phase flow boiling in a minichannel heat sink for thermal management of information and communication technology (ICT) equipment, Appl. Therm. Eng. 181 (2020), 115957.
[36] J. Zhou, X. Luo, C. Li, L. Liang, G. Wang, B. He, Z.Q. Tian, Flow boiling heat transfer enhancement under ultrasound field in minichannel heat sinks, Ultrason. Sonochem. 78 (2021), 105737.
[37] K. Enoki, M. Ono, T. Okawa, A. Akisawa, H. Mori, B. Kristiawan, A.T. Wijayanta, Two-phase flow regimes of refrigerant R134a in an oscillating horizontal rectangular minichannel conduit, Int. J. Refrig. 118 (2020) 261–268.
[38] D. Xu, Y. Fang, L. Hu, W. Yang, L. Su, Experimental investigation on thermal performance of a pumped two-phase battery cooling system using mini-channel cold plate, Int. J. Energy Res. 45 (11) (2021) 16078–16090.
[39] J. Liu, J. Liu, R. Li, X. Xu, Experimental study on flow boiling characteristics in a high aspect ratio vertical rectangular mini-channel under low heat and mass flux, Exp. Therm Fluid Sci. 98 (2018) 146–157.
[40] R. Mastrullo, A.W. Mauro, J.R. Thome, G.P. Vanoli, L. Viscito, Critical heat flux: Performance of R1234yf, R1234ze and R134a in an aluminum multi-minichannel heat sink at high saturation temperatures, Int. J. Therm. Sci. 106 (2016) 1–17.
[41] S. Saisorn, P. Wongpromma, S. Wongwises, The difference in flow pattern, heat transfer and pressure drop characteristics of mini-channel flow boiling in horizontal and vertical orientations, Int. J. Multiphase Flow. 101 (2018) 97–112.
[42] J. Zho, X. Luo, Y. Pan, D. Wan, J. Xiao, J. Zhang, B. He, Flow boiling heat transfer coefficient and pressure drop in minichannels with artificial activation cavities by direct metal laser sintering, Appl. Therm. Eng. 160 (2019), 113837.
[43] D. Jige, S. Kikuchi, N. Mikajiri, N. Inoue, Flow boiling heat transfer of zeotropic mixture R1234yf/R32 inside a horizontal multiport tube, Int. J. Refrig. 119 (2020) 390–400.
[44] J.-Y. Song, S. Hah, D. Kim, S.-M. Kim, Enhanced flow uniformity in parallel mini-channels with pin-finned inlet header, Appl. Therm. Eng. 152 (2019) 718–733.
[45] J. Xiao, X. Luo, Z. Feng, J. Zhang, Using artificial intelligence to improve identification of nanofluid gas-liquid two-phase flow pattern in mini-channel, AIP Adv. 8 (2018), 015123.
[46] S. Chen, X. Chen, G. Luo, K. Zhu, L. Chen, Y. Hou, Flow boiling instability of liquid nitrogen in horizontal mini channels, Appl. Therm. Eng. 144 (2018) 812–824.
[47] Q. Liu, B. Palm, Numerical study of bubbles rising and merging during convective boiling in micro-channels, Appl. Therm. Eng. 99 (2016) 1141–1151.
[48] M. Vermaak, J. Potgieter, J. Dirker, M.A. Moghimi, P. Valluri, K. Sefiane, J. P. Meyer, Experimental and Numerical Investigation of Micro/Mini Channel Flow-Boiling Heat Transfer with Non-Uniform Circumferential Heat Fluxes at Different Rotational Orientations, Int. J. Heat Mass Transfer. 158 (2020), 119948.
[49] P. Zhang, H.W. Jia, Evolution of flow patterns and the associated heat and mass transfer characteristics during flow boiling in mini-/micro-channels, Chem. Eng. J. 306 (2016) 978–991.
[50] B. Maciejewska, M. Piasecka, Trefftz function-based thermal solution of inverse problem in unsteady-state flow boiling heat transfer in a minichannel, Int. J. Heat Mass Transfer. 107 (2017) 925–933.
[51] H. Ma, W. Cai, J. Chen, Y. Yao, Y. Jiang, Numerical investigation on saturated boiling and heat transfer correlations in a vertical rectangular minichannel, Int. J. Therm. Sci. 102 (2016) 285–299.
[52] X. Zhang, M. Peng, T. Cong, G. Xia, A.A. Rawashdeh, Studies on the critical heat flux in fuel assembly using a modified two-phase multi-scale interface model-validation and sensitivity analysis, Int. J. Heat Mass Transfer. 176 (2021), 121443.
[53] R.K. Pal, R.K. K, Thermo-hydrodynamic modeling of flow boiling through the horizontal tube using Eulerian two-fluid modeling approach, Int. J. Heat Mass Transfer. 168 (2021) 120794.
[54] P. Liu, N. Zheng, F. Shan, Z. Liu, W. Liu, Numerical study on characteristics of heat transfer and friction factor in a circular tube with central slant rods, Int. J. Heat Mass Transfer. 99 (2016) 268–282.
[55] O. Bamigbetan, T.M. Eikevik, P. Nekså, M. Bantle, C. Schlemminger, Theoretical analysis of suitable fluids for high temperature heat pumps up to 125 °C heat delivery, Int. J. Refrig. 92 (2018) 185–195.
[56] R. Singh, T. Nguyen, M. Mochizuki, A. Akbarzadeh, Working fluid study for loop heat pipes, Therm. Sci. Eng. Prog. 35 (2022), 101451.